

Biophysical Fragment Screening of the β_1 -Adrenergic Receptor: Identification of High Affinity Arylpiperazine Leads Using Structure-Based Drug Design

John A. Christopher,^{*,†} Jason Brown,[†] Andrew S. Doré,[†] James C. Errey,[†] Markus Koglin,[†] Fiona H. Marshall,[†] David G. Myszkka,[‡] Rebecca L. Rich,[‡] Christopher G. Tate,[§] Benjamin Tehan,[†] Tony Warne,[§] and Miles Congreve[†]

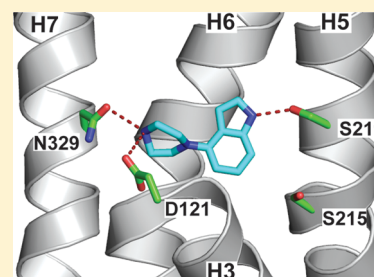
[†]Heptares Therapeutics Ltd., BioPark, Welwyn Garden City, Hertfordshire, AL7 3AX, U.K.

[‡]Biosensor Tools LLC, Salt Lake City, Utah 84103, United States

[§]MRC Laboratory of Molecular Biology, Francis Crick Avenue, Cambridge Biomedical Campus, Cambridge CB2 0QH, U.K.

S Supporting Information

ABSTRACT: Biophysical fragment screening of a thermostabilized β_1 -adrenergic receptor (β_1 AR) using surface plasmon resonance (SPR) enabled the identification of moderate affinity, high ligand efficiency (LE) arylpiperazine hits 7 and 8. Subsequent hit to lead follow-up confirmed the activity of the chemotype, and a structure-based design approach using protein–ligand crystal structures of the β_1 AR resulted in the identification of several fragments that bound with higher affinity, including indole **19** and quinoline **20**. In the first example of GPCR crystallography with ligands derived from fragment screening, structures of the stabilized β_1 AR complexed with **19** and **20** were determined at resolutions of 2.8 and 2.7 Å, respectively.



INTRODUCTION

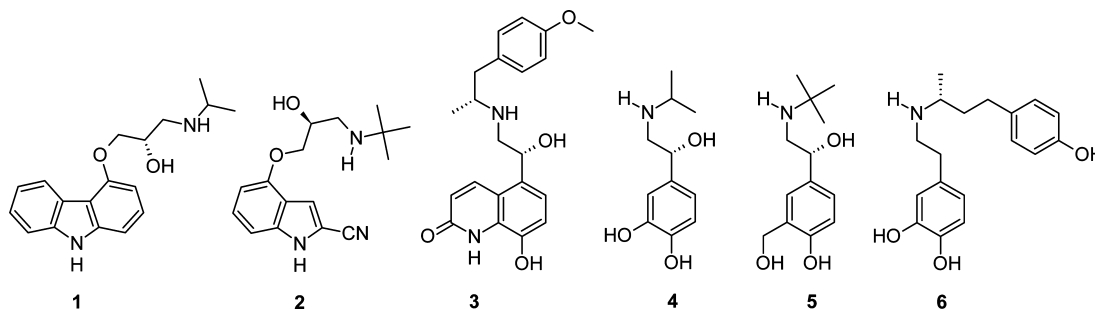
G protein-coupled receptors (GPCRs) form a large and important protein family with 390 members (excluding olfactory receptors) in the human genome.¹ GPCRs are critically involved in cell signaling in response to a wide range of endogenous ligands, including hormones, neurotransmitters, cytokines, odorants, and light. They fall into three major classes (families A, B, and C, of which family A, the rhodopsin family, is the largest). Historically, the GPCR arena has been a fruitful one for drug discovery, with a large number of small molecule drugs being successfully developed in multiple therapeutic areas, together with a smaller number of new biological entities. GPCR drug discovery continues to be an area of significant focus for the pharmaceutical industry, with over 60 new GPCR drugs, almost a quarter of the total number of approved new chemical entities (NCEs) in this period, being launched in the past 10 years.² Despite this success, only one new GPCR target per year on average has been drugged in the past decade, indicating that GPCR research remains a difficult area and one in which there are many targets with clinical relevance and validation that are currently underserved by drug discovery efforts. Historically, the vast majority of GPCR drug discovery efforts have relied upon cell-based assays coupled with high-throughput screening of large compound libraries for hit identification. This approach has resulted in limited success for challenging, clinically valuable targets such as neuropeptide receptors, chemokine receptors, family B peptide-hormone receptors and family C metabotropic glutamate (mGlu) receptors.

Until recent years, in contrast to soluble protein classes such as enzymes, X-ray crystal structures of GPCRs had been lacking with only the structure of the visual pigment rhodopsin, first reported in 2000, being available to guide structure-based drug discovery efforts.³ After a gap of 7 years, structures of the β_2 -adrenergic receptor (β_2 AR) were published,^{4,5} rapidly followed by the revelation of medium to high resolution crystal structures of 14 additional receptors (β_1 -adrenergic (β_1 AR),^{6–8} adenosine A_{2A} ,^{9,10} sphingosine 1-phosphate 1 (S1P1),¹¹ chemokine CXCR4,¹² dopamine D_3 ,¹³ histamine H_1 ,¹⁴ muscarinic acetylcholine M_2 and M_3 ,^{15,16} neurotensin,¹⁷ opioid receptors δ ,¹⁸ κ ,¹⁹ μ ,²⁰ nociceptin,²¹ and protease-activated receptor 1 (PAR1).²² It has also recently been disclosed that the first example of a family B GPCR structure, that of the corticotropin releasing factor (CRF-1) receptor, has been solved.²³ The significance of this recent upsurge in GPCR crystallographic information to drug discovery has been recently reviewed.^{24,25}

The success in obtaining new X-ray crystal structures has been due to technical advances that have stabilized purified receptors in detergent solution and locked them in specific conformations, both of which are necessary for the formation of well-diffracting crystals.^{26,27} Two key approaches to enable the determination of GPCR structures have been devised in recent years. First, insertion of the enzyme T4 lysozyme (T4L) into intracellular loop 3 (ICL3) of the receptor to promote the

Received: January 29, 2013

Published: March 21, 2013

Chart 1. β -Adrenergic Receptor Ligands 1–6

formation of crystal contacts has been used. The high resolution (2.4 Å) structure of the β_2 AR,⁵ previously solved at 3.4 Å in complex with an antibody fragment,⁴ was the first demonstration of this strategy. The T4L approach has been used in combination with the lipidic cubic phase (LCP) crystallization method. The second approach introduces a small number of point mutations into the receptor construct, significantly increasing thermostability of the protein and thereby enabling purification in the short chain detergents required for crystallization by vapor diffusion.^{28–30} Thermostabilized receptors form well-ordered crystals, as first demonstrated in the structure determination of the turkey β_1 AR at 2.7 Å resolution.⁷ The thermostabilization approach has the advantage of locking the receptor into a single homogeneous conformation, determined by the pharmacology of the ligand used in the stabilization process, greatly facilitating purification and structure determination. Stabilized receptors formed via this approach are also known as StaRs³¹ and typically contain a small number of thermostabilizing mutations, six in the case of the β_1 AR StaR (β_1 AR-m23), which is stabilized in an antagonist conformation.²⁹

Adrenergic receptors (adrenoceptors) are family A GPCRs that activate intracellular G proteins upon binding of endogenous catecholamine ligands such as adrenaline and noradrenaline.³² The adrenergic receptors are split into α and β classes, with the latter having β_1 , β_2 , and β_3 subtypes. More than 4 decades of research and development in the area of β -adrenergic receptors have resulted in a legacy of clinically important agonist and antagonist molecules with varying degrees of selectivity.³³ Antagonists of β -adrenergic receptors are frequently used in cardiovascular medicine,³⁴ as well as in other areas such as migraine and anxiety, and β -agonists are used in the treatment of asthma³⁵ and chronic obstructive pulmonary disease (COPD).³⁶

Crystal structures of the human β_2 AR^{4,5} and turkey β_1 AR⁷ in complex with the inverse agonist carazolol **1** and antagonist cyanopindolol **2**, respectively (Chart 1), were reported in 2007 and 2008. Subsequently, structures with the full agonists carmoterol **3** and isoprenaline **4** and the partial agonists salbutamol **5** and dobutamine **6** in the β_1 AR were published⁶ (Chart 1), as were structures with carazolol and the antagonist iodocyanopindolol in the same receptor.⁸ β_2 AR crystal structures with the inverse agonist ICI118,551 and agonist BI-167107, the latter in a nanobody-stabilized active state of the β_2 AR, have been published.^{37,38} More recently, structures of the stabilized β_1 AR bound to the β blockers bucindolol and carvedilol, which are classified as biased agonists because they stimulate G protein-independent signaling, have been reported.³⁹ In comparison to other β_1 AR structures, both of these ligands make additional contacts to helix 7 and

extracellular loop 2 (EL2) of the receptor, an observation that may provide an insight into the structural requirements of biased ligands. Taken together, the β_1 AR and β_2 AR structures provide a wealth of structural understanding within the β -adrenergic area, including insights into ligand–receptor interactions that impart antagonist, partial agonist, or full agonist pharmacologies.

The advent of GPCR crystal structures has initiated a new era of structure based drug design (SBDD) for this important target class. In concert with SBDD, fragment-based drug discovery (FBDD) as a strategy for identifying small (100–250 Da), efficient hit molecules is now a well established technique.^{40,41} Fragment hits, when coupled with a structural understanding of how they interact with their target protein, represent excellent starting points for medicinal chemistry, and many examples of how fragments have been successfully optimized to potent leads have been published.^{42–44} Indeed, multiple agents have been progressed into clinical trials in recent years and the first fragment-derived drug, vemurafenib, has reached the market.^{45,46} Biophysical methods such as SPR, NMR, and X-ray crystallography are among the mainstays of FBDD approaches used for soluble protein targets, but their application to the GPCR field has been highly challenging because of low expression and poor stability of the target receptor when isolated from the cell membrane. For these reasons, FBDD has been rarely utilized for GPCRs to date.⁴⁷

RESULTS AND DISCUSSION

Surface Plasmon Resonance (SPR) Fragment Screening. The engineering of StaRs with significantly increased thermostability has recently enabled fragment screening of GPCRs to be validated for the first time using a variety of biophysical and biochemical approaches. Screening of the β_1 AR and adenosine A_{2A} receptors by target-immobilized NMR screening (TINS) and SPR techniques, respectively, was reported in 2011,⁴⁸ and fragment screening of the adenosine A_{2A} receptor has been recently validated using the capillary electrophoresis (CE) approach.⁴⁹

Additionally, capture of the β_1 AR StaR and evaluation of the binding constants of small-molecule antagonists by SPR have been described,⁵⁰ and by use of this approach, a subset of the Heptaeres fragment library (approximately 650 fragments) was screened in tandem against the β_1 AR StaR and adenosine A_{2A} receptor StaR. Figure 1 shows the responses obtained from the β_1 AR surface plotted against responses from the A_{2A} receptor surface. Most responses (some of those shown in gray squares) cluster around the origin. These are the compounds that showed no significant binding to either receptor. A number of responses (also shown in gray squares) showed binding to both A_{2A} and β_1 AR. These nonselective binders track along the

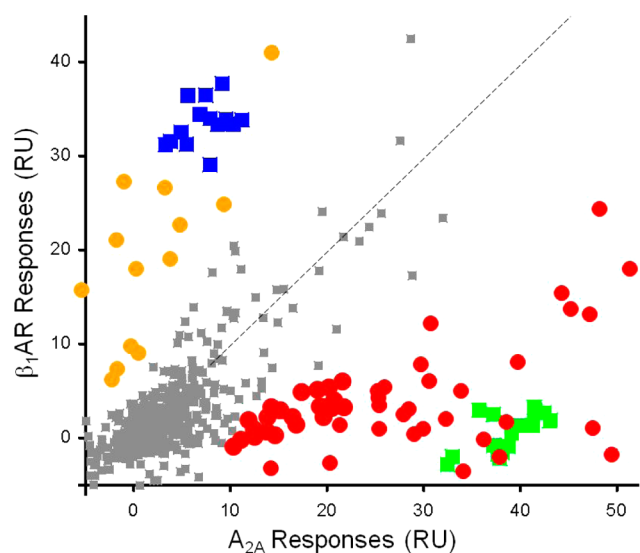


Figure 1. Plot of SPR responses of Heptares fragment library against the adenosine A_{2A} StaR and β_1 AR StaR proteins: orange circles, β_1 AR selective hits; blue squares, β_1 AR control compound; red circles, A_{2A} selective hits; green squares, A_{2A} control compound.

dashed diagonal line. Positive control compounds for each receptor were screened periodically and gave responses that cluster near the axes, confirming that these two compounds were selective binders to either β_1 AR or A_{2A} receptor. Similarly, a subset of fragments appeared to bind more significantly to one receptor or the other; hits highlighted in red were selective A_{2A} binders, those highlighted in yellow were selective β_1 AR binders. The selective β_1 AR hits were retested in concentration series to obtain affinity information. Among the selective binders to the β_1 AR StaR were 1-[3-(trifluoromethyl)phenyl]piperazine and 2-(piperazin-1-yl)quinoline (7 and 8, Chart 2), which were estimated to have encouraging binding affinities ($K_D = 16 \mu\text{M}$ ($pK_D = 4.80$) and $5.6 \mu\text{M}$ ($pK_D = 5.25$), respectively) and good ligand efficiency (LE = 0.41 and LE = 0.48, respectively).⁵¹

SAR. Substituted phenylpiperidines have ample history within GPCR drug discovery and have been described as privileged structures for this target class.⁵² The analogous phenylpiperazines also have precedent within GPCR chemical space, for example, in the atypical antipsychotics aripiprazole⁵³ and lurasidone⁵⁴ (Chart 2). Despite this significance, phenylpiperazines have little precedent in the field of β -adrenergic receptors, where the vast majority of clinically relevant molecules are typified by an ethanolamine side chain extending from an aromatic or heteroaromatic moiety (e.g., Chart 1, 1–5). Encouraged by the affinity and efficiency of SPR hits 7 and

8, we embarked upon a fragment hit-to-lead exercise to explore these phenylpiperazine fragments as novel hits for the β_1 AR.

Screening in an orthogonal assay format is a routine approach to confirm hits during FBDD, and in line with this strategy we assembled a set of commercially available analogues of similar size and complexity compared to 7 and 8 (see Modeling section). The set was screened in a radioligand membrane binding assay with human wild-type β_1 AR and [^3H]dihydroalprenolol, and affinity data (together with ligand efficiency (LE),⁵¹ ligand lipophilicity efficiency (LLE),⁵⁵ and $c\text{LogP}$ ⁵⁶ values) for selected analogues are shown in Table 1. All of the commercially available analogues tested have high ligand efficiencies and bind with moderate to high affinity. Unsubstituted phenylpiperazine 9 has good affinity, with the more polar 2-pyridyl and 2-pyrimidinyl analogues of 7 (10 and 11, respectively) being weaker and less ligand efficient than 9. Disubstituted phenyl groups yielded the highest affinities, with chloro (12–14) and methyl (15, 16) variants yielding higher affinities than the trifluoromethyl or methoxy derivatives 17 and 18. The chloro or methyl disubstituted analogues, where 2,3- or 3,5-regiochemistry is preferred over the 3,4-isomers, bound with moderate to high affinity and exceptional ligand efficiencies (>0.60). Indole 19 also has excellent affinity and ligand efficiency. Ligand lipophilicity efficiency (LLE = $pK_i - c\text{LogP}$) is another measure of druglikeness;⁵⁵ in general LLEs for the fragments are moderate to good (with the exception of the highly lipophilic 17). The LE and LLE values for several compounds in Table 1 compare favorably to those of the well characterized β_1 AR ligands carazolol 1 (LE = 0.62, LLE = 6.4), cyanopindolol 2 (LE = 0.56, LLE = 6.8), and carmoterol 3 (LE = 0.38, LLE = 5.6). Selected quinoline derivatives to explore initial SPR hit 8 were screened; 8 was included as a control and returned highly comparable affinity in the radioligand binding assay to that from the SPR screen ($pK_i = 5.20$ vs $pK_D = 5.25$, respectively). Installation of a methyl group at the 4-position (20) or substitution at the 8-position (21) yielded compounds with approximately 25-fold greater affinity than 8, whereas interchanging the methyl and piperazinyl groups of 20 to yield isomer 22 was only moderately effective. Compounds 23 and 24 were purchased to loosely mimic the carbazole core of carazolol; closer analogues were not readily available. Nevertheless, 23 and 24 returned submicromolar affinity, albeit with lower LLE than the parent hit 8. Selected compounds (12, 13, 19, and 20) were profiled in muscarinic M_1 – M_4 acetylcholine receptor membrane binding and agonist functional assays to provide an initial indication of selectivity of the piperazine fragments against related family A GPCRs. All four compounds were inactive in the functional assay for each isoform and had only weak affinity at best in the binding assays (13, 19, and 20 M_1 – M_4 $pK_i < 4.7$; 12 M_1 – M_3 $pK_i = 5.1$ – 5.4 , M_4 $pK_i = 4.5$). Further GPCR cross-screening is outside the scope of this

Chart 2. SPR Hits 7, 8, and Arylpiperazine Atypical Antipsychotics Aripiprazole and Lurasidone

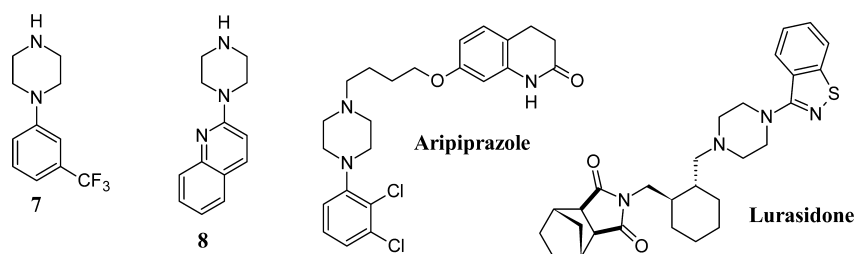
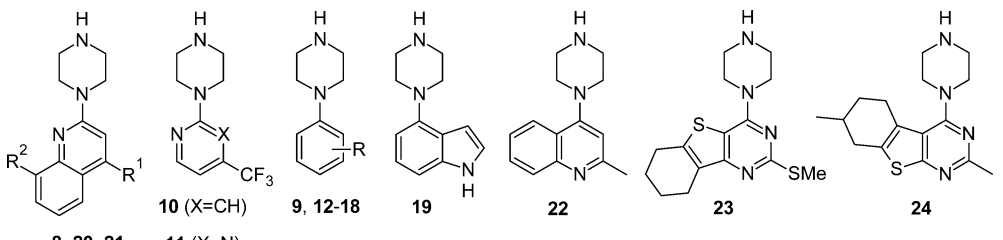


Table 1. β_1 AR Binding Affinities, LE, LLE, and cLogP Values of 8–24


compd	R, R ¹ , R ²	β_1 AR pK _i ^a	LE	cLogP ^b	LLE
8	R ¹ , R ² = H	5.20	0.44	1.59	3.61
9	R = H	5.87	0.67	1.11	4.76
10		5.63	0.48	1.51	4.12
11		5.60	0.48	1.46	4.14
12	R = 3-Cl, 5-Cl	7.07	0.69	3.03	4.04
13	R = 2-Cl, 3-Cl	6.97	0.68	2.90	4.07
14	R = 3-Cl, 4-Cl	6.67	0.65	2.67	4.00
15	R = 3-Me, 4-Me	6.13	0.60	2.03	4.10
16	R = 2-Me, 3-Me	6.27	0.61	2.03	4.24
17	R = 3-CF ₃ , 5-CF ₃	5.90	0.40	4.03	1.87
18	R = 3-OMe, 5-OMe	5.80	0.49	0.79	5.01
19		7.17	0.65	1.03	6.14
20	R ¹ = Me, R ² = H	6.65	0.53	2.05	4.60
21	R ¹ = H, R ² = 2-thienyl	6.60	0.43	2.39	4.21
22		5.80	0.47	1.44	4.36
23		6.70	0.43	3.69	3.01
24		6.17	0.40	3.06	3.11

^aSee Experimental Section for assay conditions; pK_i = $-\log_{10} K_i$. ^bReference 56.

initial communication. Given the precedent for related piperazines such as aripiprazole and lurasidone to have complex pharmacology with activities against α -adrenergic, dopaminergic, and serotonergic receptors, characterization of optimized compounds in the series against these GPCR subfamilies will be relevant.

Modeling. The advent of GPCR crystallographic information presents opportunities for structure-based design and discovery.² We sought to use the available β_1 AR crystal structure data to drive progress with the piperazine fragment hits. As it is not currently feasible to perform crystallography on the human β_1 AR because of its instability, these data were obtained with the turkey β_1 AR. However, the two receptors are 82% identical in the transmembrane and loop regions (with the exclusion of ICL3) and the residues that comprise the ligand binding pocket are 100% identical. The turkey receptor therefore provides an excellent model for studying ligand–receptor interactions.³⁹ The ligand–receptor interactions observed in the β_1 AR structures with cyanopindolol, carmoterol, and carazolol bound were of notable interest. During the hit-to-lead process, molecules were routinely docked into the liganded structure of the β_1 AR⁷ and examined in relation to inverse agonist carazolol **1**⁸ and agonist carmoterol **3**.⁶ Because of the small size of fragments and the multitude of ways they can fit into a receptor binding site, it is notoriously difficult to dock these ligands with any great confidence without examining the site in question in significant detail. A complete druggability analysis⁵⁷ of the binding site was therefore carried out to identify the region most likely to be occupied by the fragment. Water and CH aromatic probes show the regions most favorably occupied by polar and hydrophobic portions of a ligand, respectively. Optimization of overlap of the docked

molecule along with displacement of the least energetically favorable waters (shown in red in Figure 2) has been shown

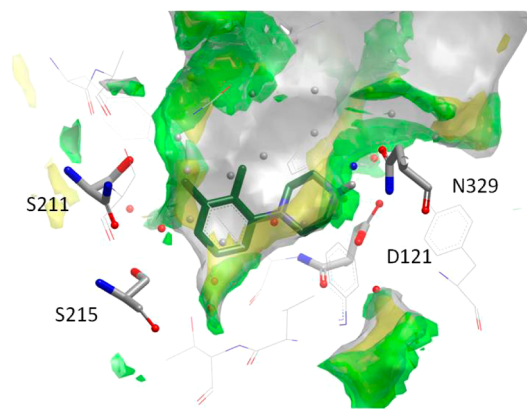


Figure 2. Druggability analysis of the β_1 AR ligand binding site,⁵⁷ showing water molecules and their energies relative to bulk solvent (red, high; blue, low) combined with surfaces depicting water probe (green) and CH aromatic probe (yellow) hotspots, with the docking pose of **16** selected for comparison to the crystal structures.

previously to be predictive for highly ligand efficient molecules.⁵⁷ Thus, this strategy was also used in our analysis of the solutions obtained from dockings, as described below in further detail for representative hit **16**. Additional compounds were selected from similarity and substructure searching approaches to complement the structure-based strategy and expand SAR in the series.

In the dockings of **16** with carazolol **1** and carmoterol **3** the carbon atom of the 3-methyl substituent of **16** overlays clearly

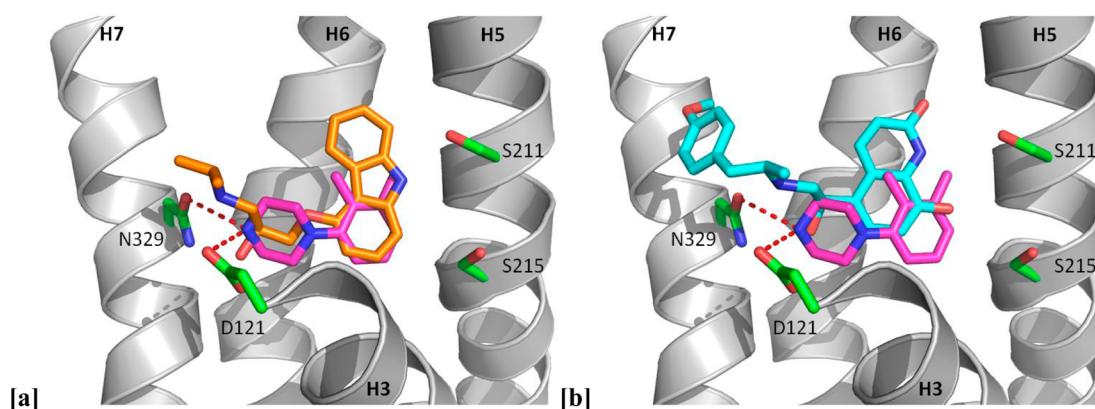


Figure 3. Piperazine **16** (pink carbons) docked into the crystal structures of (a) β_1 AR complexed with the inverse agonist carazolol **1** (orange carbons) (PDB code 2YCW)⁸ and (b) β_1 AR complexed with the agonist carmoterol **3** (cyan carbons) (PDB code 2Y02).⁶

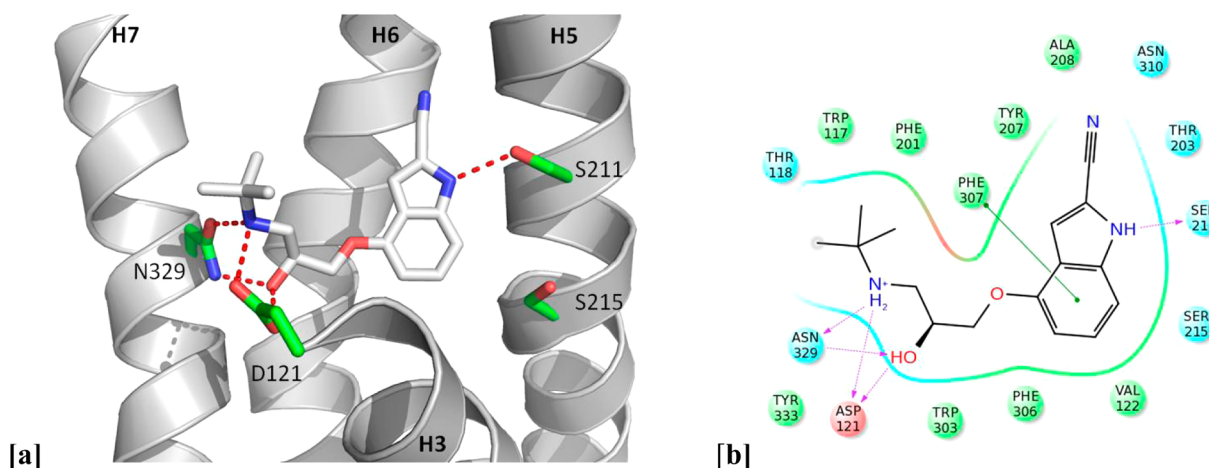


Figure 4. (a) X-ray crystal structure of the antagonist cyanopindolol **2** in complex with β_1 AR (PDB code 2VT4).⁷ (b) Key interactions between **2** and β_1 AR. Residues in green spheres are hydrophobic. Blue spheres are polar, and red spheres are negatively charged. The purple arrows and their directions represent hydrogen bonds between the ligand and the protein. The green line represents the π - π stacking arrangement seen between the aromatic core and the aromatic residue Phe307.^{6,52}

with the carbazole nitrogen of **1** and is in the region of the quinolinone nitrogen of **3**, suggesting an opportunity to introduce similar polar interactions with the receptor in this area of the molecule (Figure 3). This possibility is more clearly visualized in the structure of cyanopindolol **2** in the β_1 AR stabilized receptor⁷ (Figure 4), where hydrogen bond donation of the indole nitrogen to Ser211^{5,42} (superscripts indicate Ballesteros–Weinstein nomenclature⁵⁸), a nonpolar interaction of the indole phenyl ring with Phe307^{6,52}, and interaction of the charged ethanolamine portion with Asp121^{3,32} and Asn329^{7,39} are observed. Inspired by these observations, we extended our studies to include a number of molecules with larger and more polar substituents in order to promote further interactions with residues in the β_1 AR ligand binding site and in particular polar interactions with Ser211 on helix 5. The strategy most notably resulted in identification of the simple indole derivative **19** (Table 1), which has both high affinity and ligand efficiency and reduced lipophilicity compared to parent molecule **16**, a finding that validated our structure-driven approach and represents a very promising lead compound for further optimization.

Crystal Structures of β_1 AR Bound to Fragments 19 and 20. The identification of a series of piperazine-based fragments with high affinity and high solubility⁵⁹ provided an invaluable opportunity to obtain co-structures of the molecules

with the β_1 AR, as detailed structural information would confirm the modes of binding of the fragments, facilitate comparisons with existing structures, and indicate opportunities for further development. On the basis of a consideration of affinity and ligand efficiency, indole **19** and the structurally dissimilar quinoline **20** were selected for crystallography trials. Cococrystallization of thermostabilized β_1 AR with fragments **19** and **20** was performed as previously described^{6,39} and resulted in structures determined to resolutions of 2.8 and 2.7 Å, respectively (Supporting Information Table 2). The structures show that the piperazine rings in the two molecules are located between Asp121^{3,32} on helix 3 (H3) and Asn329^{7,39} on H7, and their phenyl substituents are positioned adjacent to H5 (Figure 5a and Figure 5b). The piperazine ring therefore substitutes for the ethanolamine core of conventional adrenergic receptor ligands, and the structural roles of the phenyl substituents are similar to those of the indolecarbonitrile and carbazole headgroups of cyanopindolol and carazolol (Figure 5c and Figure 5d). However, the total number and nature of ligand–receptor interactions observed in the β_1 AR-**19** and β_1 AR-**20** structures are reduced when compared to those observed in the crystal structures with cyanopindolol⁷ and carazolol⁸ (Supporting Information Table 3). With cyanopindolol and carazolol, the ethanolamine secondary amine and β -hydroxyl groups both

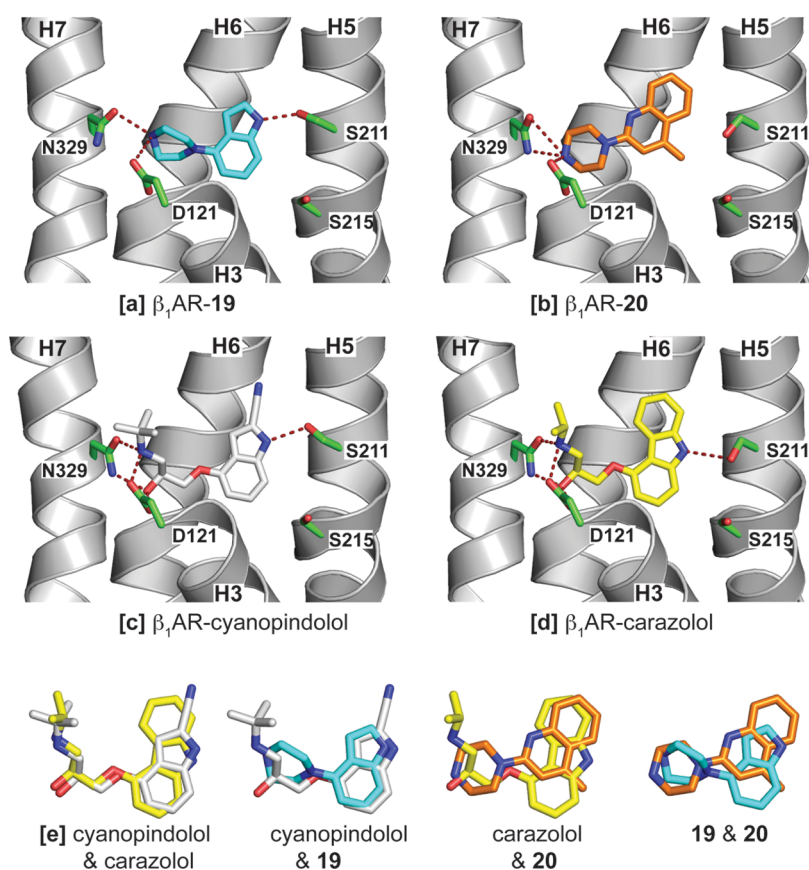


Figure 5. β_1 AR structures are shown in cartoon representation as viewed in the membrane plane with all or part of H1, H2, H3, and H4 obscuring the ligand binding site removed for clarity, and the extracellular side is uppermost: (a) β_1 AR-19; (b) β_1 AR-20; (c) β_1 AR-cyanopindolol (PDB code 2VT4);⁷ (d) β_1 AR-carazolol (PDB code 2YCW).⁸ Atoms are colored accordingly. For ligands/fragments: C, cyan, gold, silver, yellow; O, red; N, blue. For selected receptor side chains: C, green; O, red; N, blue. Potential hydrogen bonds and polar contacts are shown as red dashes. For a full list of receptor–ligand interactions see Supporting Information Table 3. (e) Superposition of ligand positions after alignment of the β_1 AR structures. Global alignment of the receptor structures (monomers selected as in Supporting Information Table 3) was performed using Pymol (superpose), and the resulting positions of the ligands are depicted.

form hydrogen bonds to the Asp121^{3,32} and Asn329^{7,39} side chains. In contrast, with **19** and **20**, only one secondary amine nitrogen in the piperazine ring is suitably positioned to interact with Asp121^{3,32} and Asn329^{7,39}, and the interactions are mostly weaker, polar interactions rather than hydrogen bonds (Supporting Information Table 3). Possibly as a consequence of the weaker interactions of fragments **19** and **20**, there is greater variation in the orientation of the piperazine rings than is shown by the ethanolamine groups in carazolol and cyanopindolol. This can be observed in the superpositions of the different ligands and fragments complexed with the receptor depicted in Figure 5e. The variation in the positions of the piperazine rings in the two structures results in some differences in how **19** and **20** interact with Asp121^{3,32}, Asn329^{7,39}, Trp303^{6,48}, and Tyr333^{7,43} (Supporting Information Table 3). The structures of β_1 AR bound to **19** and **20** do not show either the change in rotamer conformation of Ser215^{5,46} observed when full agonists are bound⁶ or a contraction of the ligand binding pocket (Supporting Information Table 3) characteristic of the binding of both full and partial agonists.⁶ These observations suggest that both of the fragments are antagonists, although data to support this hypothesis have not yet been generated. However, the interactions of the phenyl substituent headgroup with Ser211^{5,42} on H5 differ between the two fragment molecules, as only **19** can form a hydrogen bond

to Ser211^{5,42}. In the β_1 AR-**20** structure, the conformation of Ser211^{5,42} is similar to that observed in the β_1 AR-carazolol structure (Figure 5b and Figure 5d), whereas in the β_1 AR-**19** structure the conformation of Ser211^{5,42} corresponds to that observed in the β_1 AR-cyanopindolol structure (Figure 5a and Figure 5c). The differences in pharmacological activity between cyanopindolol (a partial agonist with sympathomimetic activity) and carazolol (an inverse agonist) may in part result from the differences in the conformation of Ser211^{5,42} observed in the structures with these ligands⁶⁰ (Figure 5c and Figure 5d), and there may be similar differences in pharmacological activity between **19** and **20**. Because of their relatively small size, fragments **19** and **20** interact with a subset of the residues that comprise the ligand binding pocket. This suggests that by use of the detailed structural information that has been made available, the targeted addition of further substituents to these fragments could serve to further increase their affinities, as well as to modulate their pharmacological activities.

CONCLUSIONS

Fragment screening is a well-established and powerful approach to the discovery of a new lead series that is now starting to be utilized for membrane-bound receptor targets. Recent virtual screening efforts have demonstrated that, at least for aminergic family A GPCRs, fragment hits can be identified, now that the

details of how small molecules bind to these receptors are better understood.^{61–64} Furthermore, studies on, for example, the histamine H₁ receptor (H₁R) have shown, in a manner analogous to the work exemplified here, that fragment-sized ligands can be bound to the receptor, crystallized and their binding modes established.⁶⁵ In the research presented here, biophysical fragment screening of β_1 AR using SPR was enabled by receptor stabilization and led to the identification of arylpiperazine hits 7 and 8. Selection of analogues for screening in an orthogonal wild-type radioligand membrane binding assay through similarity and substructural searching approaches was complemented by the use of β -adrenergic receptor crystallographic information, allowing a parallel structure-based design strategy. High affinity and ligand efficient fragments were identified, including indole 19 and quinoline 20, which were identified and subsequently cocrystallized with the stabilized β_1 AR, yielding structures at 2.8 and 2.7 Å, respectively. Overall, these results demonstrate, for the first time, that a true fragment based drug discovery paradigm, encompassing biophysical screening with a direct-binding platform of a diverse fragment library, structure-guided fragment optimization, and cocrystallization of fragment hits, can now be applied to GPCR targets.

■ EXPERIMENTAL SECTION

Expression of β_1 AR and Membrane Preparation. HEK293 cells were transiently transfected with cDNA encoding human β_1 AR using Genejuice (Novagen) according to the manufacturer's instructions to achieve approximately 2×10^9 post-transfected cells. After 48 h of incubation the cells were dissociated using TrypLE Express cell dissociation fluid and washed with PBS, pelleted down, and stored at -80°C until required. The pellet was resuspended in chilled buffer consisting of 20 mM HEPES, 10 mM EDTA containing 1× Complete protease inhibitor cocktail tablet per 50 mL of buffer (pH 7.4). All subsequent procedures were carried out at 4°C . The suspension was homogenized for 15 s and centrifuged at 40000g for 15 min. The pellet was suspended in buffer containing 20 mM HEPES and 0.1 mM EDTA (pH 7.4) and homogenized for 30 s. After centrifugation at 40000g for 45 min, the pellet was resuspended in the same buffer and homogenized for a further 30 s. Protein concentration was estimated against the standard bovine serum albumin using the BCA method (Pierce, Socochim, Lausanne, Switzerland) and then frozen to -80°C at 2 mg/mL prior to use.

β_1 AR Radioligand Binding Assay. Cell membranes were incubated with [³H]dihydroalprenolol in assay buffer (50 mM HEPES, 15 mM MgCl₂, 150 mM NaCl, pH 7.4) in a total assay volume of 0.25 mL with a final DMSO concentration of 1%. After 90 min of incubation at room temperature the reaction was terminated by rapid filtration through GF/B 96-well glass fiber plates with 5×0.25 mL washes with doubly distilled H₂O using a Tomtec cell harvester. Bound radioactivity was determined through liquid scintillation using Lablogic SafeScint and detected on a MicroBeta liquid scintillation counter. Nonspecific binding was determined as that remaining in the presence of a 10 μM saturating concentration of the antagonist alprenolol. Competition binding was performed by incubating membranes (1.25 μg of protein/well) with 1.5 nM [³H]-dihydroalprenolol and a range of concentrations of the test compound. IC₅₀ values were derived from fitting to a four-parameter logistic equation in PRISM (GraphPad Software, San Diego, CA, U.S.). Apparent K_i values were derived using the equation of Cheng and Prusoff.⁶⁶ Binding affinities are expressed as pK_i values, where pK_i = $-\log_{10} K_i$.

SPR Experimental Details. Surface plasmon resonance (SPR) binding studies were performed at 25°C using Biacore T200 and S51 optical biosensors equipped with nickel-charged NTA chips and equilibrated with running buffer (20 mM Tris-HCl, 350 mM NaCl, 0.1% dodecylmaltoside, 5% DMSO, pH 7.8). Aliquots of the affinity-purified, His-tagged β_1 AR and A_{2A} receptors were both capture-

coupled⁵⁰ on the sensor surface to densities of >9000 resonance units (RU). In an initial screen, the entire library was tested at 50 μM with two control compounds, L-748,337 (a β_1 AR positive control, CAS 244192-94-7) and PSB 1115 (an A_{2A} receptor positive control, CAS 409344-71-4), tested periodically at 10 μM throughout the screen to track the activity of the receptor surfaces. For a second screen, fresh receptor surfaces were prepared and the compound library was retested at 11 μM (after omitting compounds that bound to the reference surface or bound with nanomolar affinity to A_{2A}). Again, the positive controls were tested periodically throughout the screen. Potential selective β_1 AR hits were analyzed in concentration series (2-fold dilutions typically starting at 150 μM , with each concentration tested in duplicate) to confirm their selectivity and determine their affinities.

Computational Chemistry. The crystal structure of β_1 AR bound with cyanopindolol, PDB code 2VT4,⁷ was used as the basis for dockings of fragments. Protein preparation and docking experiments were done within the Schrodinger Maestro package.⁶⁷ The protein preparation workflow was used to add hydrogens, cap the N-terminus and C-terminus groups, optimize the orientation of hydroxyl groups, Asn, and Gln, and the protonation state of His, and then perform a number of constrained refinements on the hydrogens alone and the protein with a maximum rmsd tolerance of 0.30 Å. Dockings were undertaken using the Glide extra precision (XP) protocol within Maestro. GRID analyses of the binding sites were used to evaluate potential docking poses and drive the designs (using the Csp3 probe (C3) for shape, aromatic CH probe (C1=) for lipophilic hotspots, water probe (OH₂) for water hotspots, carbonyl group probe (O) for hydrogen bond acceptor hotspots, and amide NH probe (N1) for hydrogen-bond donor hotspots).^{68,69} Similarity and substructure searches were conducted within Canvas from Schrodinger.⁶⁷ The MolPrint2D algorithm as implemented in Canvas was used for the similarity searching.⁷⁰

Expression, Purification, and Crystallization of Thermo-stabilized β_1 AR. The turkey (*Meleagris gallopavo*) β_1 AR (StaR) construct that was used in crystallization experiments, β_44 -m23, contains six thermostabilizing point mutations and truncations at the N terminus, inner loop 3, and C terminus.^{6,71} Receptor expression in insect cells and purification were all performed as described previously.^{71,72} For crystallization, the detergent was exchanged to Hega-10 (0.35%) on an alprenolol affinity column. Receptor was competitively eluted from the alprenolol affinity column with 100 μM ligand (19 or 20) and concentrated to 25 mg/mL in 10 mM Tris-HCl, pH 7.6, 100 mM NaCl, 0.1 mM EDTA, 0.35% Hega-10. Before crystallization, Hega-10 and cholesteryl hemisuccinate were added to 0.5% and 1 mg/mL respectively. Crystals were grown at 4°C by vapor diffusion in sitting drops with 150 nL of receptor + 150 nL of precipitant (0.1 M bicine, pH 9.0, 24% PEG 600 in both cases) and cryoprotected by addition of 60% PEG 600 for 1 min before mounting on Hampton CrystalCap HT loops and cryocooling in liquid nitrogen.

Data Collection, Structure Solution, and Refinement. For both β_1 AR-19 and β_1 AR-20 structures, diffraction data were collected from a single cryocooled crystal (100 K) using a 10 μm focused beam at I24, Diamond Light Source, Oxford, U.K. Images were processed with MOSFLM⁷³ and SCALA.⁷⁴ Both structures were solved by molecular replacement with Phaser⁷⁵ using the structure of β_1 AR with carvedilol bound (PDB code 4AMJ³⁹) as a starting model. Refinement, rebuilding, and validation were carried out with REFMAC5,⁷⁶ Coot,⁷⁷ and MolProbity.⁷⁸ In both the β_1 AR-19 and β_1 AR-20 structures there is a distortion of the ligand binding pocket in monomer A due to lattice contacts, and monomer B represents the more physiologically relevant conformation. The β_1 AR-19 and β_1 AR-20 crystal structures were determined at a resolution of 2.8 and 2.7 Å, respectively. This resolution was more than adequate to provide clear omit electron densities that enabled unequivocal placement of the ligands in the structures (Supporting Information Figure 1), as well as further details such as specifically bound detergent and lipid molecules and ordered internal water molecules and sodium ions (Supporting Information Table 2).

■ ASSOCIATED CONTENT

Supporting Information

Supplier information and LCMS QC data for all compounds, NMR data for selected compounds, muscarinic M₁–M₄ acetylcholine receptor membrane binding and agonist functional assay data for compounds **12**, **13**, **19**, and **20**, and crystallographic information tables (data processing, refinement and evaluation statistics, ligand–receptor interactions, and ligand binding pocket dimensions) and omit maps for the ligands **19** and **20** in the crystal structures. This material is available free of charge via the Internet at <http://pubs.acs.org>.

Accession Codes

Coordinates and structure factors have been submitted to the PDB under accession codes 3ZPQ and 3ZPR for β_1 AR bound to **19** and **20**, respectively.

■ AUTHOR INFORMATION

Corresponding Author

*Phone: +44 (0)1707 358731. Fax: +44 (0)1707 358640. E-mail: john.christopher@heptares.com.

Notes

The authors declare no competing financial interest.

■ ACKNOWLEDGMENTS

We thank Edward Hurrell and Greg Osborne for generation of data in the muscarinic M₁–M₄ acetylcholine receptor membrane binding and agonist functional assays, and Andrew Green for assistance with generation of β_1 AR binding data. Work by TW and CGT was supported by core funding from the Medical Research Council (MRC U105197215) and a BBSRC grant (BB/G003653/1).

■ ABBREVIATIONS USED

β_1 AR, β_1 -adrenergic receptor; CE, capillary electrophoresis; GPCR, G-protein-coupled receptor; Hega-10, decanoyl-N-hydroxyethylglucamide; HEPES, (4-(2-hydroxyethyl)-1-piperazineethanesulfonic acid; T4L, T4 lysozyme; LCP, lipidic cubic phase; StaR, stabilized receptor; SPR, surface plasmon resonance; TINS, target immobilized NMR screening; LLE, ligand-lipophilicity efficiency

■ REFERENCES

- (1) Lagerström, M. C.; Schiöth, H. B. Structural diversity of G protein-coupled receptors and significance for drug discovery. *Nat. Rev. Drug Discovery* **2008**, *7*, 339–357.
- (2) Congreve, M.; Langmead, C.; Mason, J.; Marshall, F. Progress in structure based drug design for G protein-coupled receptors. *J. Med. Chem.* **2011**, *54*, 4283–4311.
- (3) Palczewski, K.; Kumasaka, T.; Hori, T.; Behnke, C. A.; Motoshima, H.; Fox, B. A.; Le Trong, I.; Teller, D. C.; Okada, T.; Stenkamp, R. E.; Yamamoto, M.; Miyano, M. Crystal structure of rhodopsin: a G protein-coupled receptor. *Science* **2000**, *289*, 739–745.
- (4) Rasmussen, S. G. F.; Choi, H.-J.; Rosenbaum, D. M.; Kobilka, T. S.; Thian, F. S.; Edwards, P. C.; Burghammer, M.; Ratnala, V. R. P.; Sanishvili, R.; Fischetti, R. F.; Schertler, G. F. X.; Weis, W. I.; Kobilka, B. K. Crystal structure of the human β_2 adrenergic G-protein-coupled receptor. *Nature* **2007**, *450*, 383–387.
- (5) Cherezov, V.; Rosenbaum, D. M.; Hanson, M. A.; Rasmussen, S. G.; Thian, F. S.; Kobilka, T. S.; Choi, H. J.; Kuhn, P.; Weis, W. I.; Kobilka, B. K.; Stevens, R. C. High-resolution crystal structure of an engineered human β_2 -adrenergic G protein-coupled receptor. *Science* **2007**, *318*, 1258–1265.
- (6) Warne, T.; Moukhametzianov, M.; Baker, J. G.; Nehmé, R.; Edwards, P. C.; Leslie, A. G. W.; Schertler, G. F. X.; Tate, C. G. The

structural basis for agonist and partial agonist action on a β_1 -adrenergic receptor. *Nature* **2011**, *469*, 241–244.

- (7) Warne, T.; Serrano-Vega, M. J.; Baker, J. G.; Moukhametzianov, R.; Edwards, P. C.; Henderson, R.; Leslie, A. G. W.; Tate, C. G.; Schertler, G. F. X. Structure of a β_1 -adrenergic G-protein-coupled receptor. *Nature* **2008**, *454*, 486–491.

- (8) Moukhametzianov, R.; Warne, T.; Edwards, P. C.; Serrano-Vega, M. J.; Leslie, A. G. W.; Tate, C. G.; Schertler, G. F. X. Two distinct conformations of helix 6 observed in antagonist-bound structures of a β_1 -adrenergic receptor. *Proc. Natl. Acad. Sci. U.S.A.* **2011**, *108*, 8228–8232.

- (9) Jaakola, V. P.; Griffith, M. T.; Hanson, M. A.; Cherezov, V.; Chien, E. Y.; Lane, J. R.; Ijzerman, A. P.; Stevens, R. C. The 2.6 angstrom crystal structure of a human A_{2A} adenosine receptor bound to an antagonist. *Science* **2008**, *322* (5905), 1211–1217.

- (10) Xu, F.; Wu, H.; Katritch, V.; Han, G. W.; Jacobson, K. A.; Gao, Z.-G.; Cherezov, V.; Stevens, R. C. Structure of an agonist-bound human A_{2A} adenosine receptor. *Science* **2011**, *332*, 322–327.

- (11) Hanson, M. A.; Roth, C. B.; Jo, E.; Griffith, M. T.; Scott, F. L.; Reinhart, G.; Desale, H.; Clemons, B.; Cahalan, S. M.; Schuerer, S. C.; Sanna, M. G.; Han, G. W.; Kuhn, P.; Rosen, H.; Stevens, R. C. Crystal structure of a lipid G protein-coupled receptor. *Science* **2012**, *335*, 851–855.

- (12) Wu, B.; Chien, E. Y.; Mol, C. D.; Fenalti, G.; Liu, W.; Katritch, V.; Abagyan, R.; Brooun, A.; Wells, P.; Bi, F. C.; Hamel, D. J.; Kuhn, P.; Handel, T. M.; Cherezov, V.; Stevens, R. C. Structures of the CXCR4 chemokine GPCR with small-molecule and cyclic peptide antagonists. *Science* **2010**, *330*, 1066–1071.

- (13) Chien, E. Y.; Liu, W.; Zhao, Q.; Katritch, V.; Han, G. W.; Hanson, M. A.; Shi, L.; Newman, A. H.; Javitch, J. A.; Cherezov, V.; Stevens, R. C. Structure of the human dopamine D₃ receptor in complex with a D₂/D₃ selective antagonist. *Science* **2010**, *330*, 1091–1095.

- (14) Shimamura, T.; Shiroishi, M.; Weyand, S.; Tsujimoto, H.; Winter, G.; Katritch, V.; Abagyan, R.; Cherezov, V.; Liu, W.; Han, G. W.; Kobayashi, T.; Stevens, R. C.; Iwata, S. Structure of the human histamine H₁ receptor complex with doxepin. *Nature* **2011**, *475*, 65–70.

- (15) Haga, K.; Kruse, A. C.; Asada, H.; Yurugi-Kobayashi, T.; Shiroishi, M.; Zhang, C.; Weis, W. I.; Okada, T.; Kobilka, B. K.; Haga, T.; Kobayashi, T. Structure of the human M₂ muscarinic acetylcholine receptor bound to an antagonist. *Nature* **2012**, *482*, 547–551.

- (16) Kruse, A. C.; Hu, J.; Pan, A. C.; Arlow, D. H.; Rosenbaum, D. M.; Rosemond, E.; Green, H. F.; Liu, T.; Chae, P. S.; Dror, R. O.; Shaw, D. E.; Weis, W. I.; Wess, J.; Kobilka, B. K. Structure and dynamics of the M₃ muscarinic acetylcholine receptor. *Nature* **2012**, *482*, 552–556.

- (17) White, J. F.; Noinaj, N.; Shibata, Y.; Love, J.; Kloss, B.; Xu, F.; Gvozdenovic-Jermic, J.; Shah, P.; Shiloach, J.; Tate, C. G.; Grishammer, R. Structure of the agonist-bound neurotensin receptor. *Nature* **2012**, *490*, 508–513.

- (18) Granier, S.; Manglik, A.; Kruse, A. C.; Kobilka, T. S.; Thian, F. S.; Weis, W. I.; Kobilka, B. K. Structure of the δ -opioid receptor bound to naltrindole. *Nature* **2012**, *485*, 400–404.

- (19) Wu, H.; Wacker, D.; Mileni, M.; Katritch, V.; Han, G. W.; Vardy, E.; Liu, W.; Thompson, A. A.; Huang, X. P.; Carroll, F. L.; Mascarella, S. W.; Westkaemper, R. B.; Mosier, P. D.; Roth, B. L.; Cherezov, V.; Stevens, R. C. Structure of the human κ -opioid receptor in complex with JDTic. *Nature* **2012**, *485*, 327–332.

- (20) Manglik, A.; Kruse, A. C.; Kobilka, T. S.; Thian, F. S.; Mathiesen, J. M.; Sunahara, R. K.; Pardo, L.; Weis, W. I.; Kobilka, B. K.; Granier, S. Crystal structure of the μ -opioid receptor bound to a morphinan antagonist. *Nature* **2012**, *485*, 321–326.

- (21) Thompson, A. A.; Liu, W.; Chun, E.; Katritch, V.; Wu, H.; Vardy, E.; Huang, X. P.; Trapella, C.; Guerrini, R.; Calo, G.; Roth, B. L.; Cherezov, V.; Stevens, R. C. Structure of the nociceptin/orphanin FQ receptor in complex with a peptide mimetic. *Nature* **2012**, *485*, 395–399.

- (22) Zhang, C.; Srinivasan, Y.; Arlow, D. H.; Fung, J. J.; Palmer, D.; Zheng, Y.; Green, H. F.; Pandey, A.; Dror, R. O.; Shaw, D. E.; Weis, W. I.; Coughlin, S. R.; Kobilka, B. K. High-resolution crystal structure of human protease-activated receptor 1. *Nature* **2012**, *492*, 387–392.
- (23) Heptares Therapeutics Ltd. press release. <http://www.heptares.com/news/65/74/Heptares-Solves-First-Family-B-GPCR-Structure.html> (accessed March 6, 2013).
- (24) Salon, J. A.; Lodowski, D. T.; Palczewski, K. The significance of G protein-coupled receptor crystallography for drug discovery. *Pharmacol. Rev.* **2011**, *63*, 901–937.
- (25) Hanson, M. A.; Stevens, R. C. Discovery of new GPCR biology: one receptor structure at a time. *Structure* **2009**, *17*, 8–14.
- (26) Tate, C. G.; Schertler, G. F. X. Engineering G protein-coupled receptors to facilitate their structure determination. *Curr. Opin. Struct. Biol.* **2009**, *19*, 383–395.
- (27) Tate, C. G. A crystal clear solution for determining G-protein-coupled receptor structures. *Trends Biochem. Sci.* **2012**, *37*, 343–352.
- (28) Magnani, F.; Shibata, Y.; Serrano-Vega, M. J.; Tate, C. G. Co-evolving stability and conformational homogeneity of the human adenosine A_{2a} receptor. *Proc. Natl. Acad. Sci. U.S.A.* **2008**, *105*, 10744–10749.
- (29) Serrano-Vega, M. J.; Magnani, F.; Shibata, Y.; Tate, C. G. Conformational thermostabilisation of the β_1 -adrenergic receptor in a detergent-resistant form. *Proc. Natl. Acad. Sci. U.S.A.* **2008**, *105*, 877–882.
- (30) Shibata, Y.; White, J. F.; Serrano-Vega, M. J.; Magnani, F.; Aloia, A. L.; Grishammer, R.; Tate, C. G. Thermostabilisation of the neurotensin receptor NTS1. *J. Mol. Biol.* **2009**, *390*, 262–277.
- (31) Robertson, N.; Jazayeri, A.; Errey, J.; Baig, A.; Hurrell, E.; Zhukov, A.; Langmead, C. J.; Weir, M.; Marshall, F. H. The properties of thermostabilised G protein-coupled receptors (StaRs) and their use in drug discovery. *Neuropharmacology* **2011**, *60*, 36–44.
- (32) Evans, B. A.; Sato, M.; Sarwar, M.; Hutchinson, D. S.; Summers, R. J. Ligand-directed signalling at β -adrenoceptors. *Br. J. Pharmacol.* **2010**, *159*, 1022–1038.
- (33) Baker, J. G. The selectivity of β -adrenoceptor antagonists at the human β_1 , β_2 and β_3 adrenoceptors. *Br. J. Pharmacol.* **2005**, *144*, 317–322.
- (34) Zheng, M.; Zhu, W.; Han, Q.; Xiao, R.-P. Emerging concepts and therapeutic implications of β -adrenergic receptor subtype signalling. *Pharmacol. Ther.* **2005**, *108*, 257–268.
- (35) Hospenthal, M. A. C.; Peters, J. I. Long-acting β_2 -agonists in the management of asthma exacerbations. *Curr. Opin. Pulm. Med.* **2005**, *11*, 69–73.
- (36) Schachter, E. N. New β_2 -adrenoceptor agonists for the treatment of chronic obstructive pulmonary disease. *Drugs Today* **2010**, *46*, 911–918.
- (37) Wacker, D.; Fenalti, G.; Brown, M. A.; Katritch, V.; Abagyan, R.; Cherezov, V.; Stevens, R. C. Conserved binding mode of human β_2 adrenergic receptor inverse agonists and antagonist revealed by X-ray crystallography. *J. Am. Chem. Soc.* **2010**, *132*, 11443–11445.
- (38) Rasmussen, S. G. F.; Choi, H.-J.; Fung, J. J.; Pardon, E.; Casarosa, P.; Chae, P. S.; DeVree, B. T.; Rosenbaum, D. M.; Thian, F. S.; Kobilka, T. S.; Schnapp, A.; Konetzki, I.; Sunahara, R. K.; Gellman, S. H.; Pautsch, A.; Steyaert, J.; Weis, W. I.; Kobilka, B. K. Structure of a nanobody-stabilized active state of the β_2 adrenoceptor. *Nature* **2011**, *469*, 175–180.
- (39) Warne, T.; Edwards, P. C.; Leslie, A. G. W.; Tate, C. G. Crystal structures of a stabilized β_1 -adrenoceptor bound to the biased agonists bucindolol and carvedilol. *Structure* **2012**, *20*, 841–849.
- (40) Myszk, D.; Paul, J. Exploring the horizons of small molecule drug discovery: the evolution and application of the ideal fragment library. *Drug Discovery World* **2011/12**, Winter, 51–58.
- (41) Erlanson, D. A. Introduction to fragment-based drug discovery. *Top. Curr. Chem.* **2012**, *317*, 1–32.
- (42) Congreve, M.; Chessari, G.; Tisi, D.; Woodhead, A. J. Recent developments in fragment-based drug discovery. *J. Med. Chem.* **2008**, *51*, 3661–3680.
- (43) Chessari, G.; Woodhead, A. J. From fragment to clinical candidate—a historical perspective. *Drug Discovery Today* **2009**, *14*, 668–675.
- (44) Schulz, M. N.; Hubbard, R. E. Recent progress in fragment-based lead discovery. *Curr. Opin. Pharmacol.* **2009**, *9*, 615–621.
- (45) Bollag, G.; Tsai, J.; Zhang, J.; Zhang, C.; Ibrahim, P.; Nolop, K.; Hirth, P. Vemurafenib: the first drug approved for BRAF-mutant cancer. *Nat. Rev. Drug Discovery* **2012**, *11*, 873–886.
- (46) Tsai, J.; Lee, J. T.; Wang, W.; Zhang, J.; Cho, H.; Mamo, S.; Bremer, R.; Gillette, S.; Kong, J.; Haass, N. K.; Sproesser, K.; Li, L.; Smalley, K. S. M.; Fong, D.; Zhu, Y.-L.; Marimuthu, A.; Nguyen, H.; Lam, B.; Liu, J.; Cheung, I.; Rice, J.; Suzuki, Y.; Luu, C.; Settachatgul, C.; Shellooe, R.; Cantwell, J.; Kim, S.-H.; Schlessinger, J.; Zhang, K. Y. J.; West, B. L.; Powell, B.; Habets, G.; Zhang, C.; Ibrahim, P. N.; Hirth, P.; Artis, D. R.; Herlyn, M.; Bollag, G. Discovery of a selective inhibitor of oncogenic B-Raf kinase with potent antimelanoma activity. *Proc. Natl. Acad. Sci. U.S.A.* **2008**, *105*, 3041–3046.
- (47) Albert, J. S.; Blomberg, N.; Breeze, A. L.; Brown, A. J.; Burrows, J. N.; Edwards, P. D.; Folmer, R. H.; Geschwindner, S.; Griffen, E. J.; Kenny, P. W.; Nowak, T.; Olsson, L. L.; Sanganee, H.; Shapiro, A. B. An integrated approach to fragment-based lead generation: philosophy, strategy and case studies from AstraZeneca's drug discovery programmes. *Curr. Top. Med. Chem.* **2007**, *7*, 1600–1629.
- (48) Congreve, M.; Rich, R. L.; Myszk, D. G.; Figaroa, F.; Siegal, G.; Marshall, F. H. Fragment Screening of Stabilized G-Protein-Coupled Receptors Using Biophysical Methods. In *Methods in Enzymology*, Vol. 493; Kuo, L. C., Ed.; Academic Press: Burlington, MA, U.S.A., 2011; pp 115–136.
- (49) Andrews, S. P.; Tehan, B. Stabilised G protein-coupled receptors in structure-based drug design: a case study with adenosine A_{2a} receptor. *Med. Chem. Commun.* **2013**, *4*, 52–67.
- (50) Rich, R. L.; Errey, J.; Marshall, F.; Myszk, D. G. Biacore analysis with stabilized G-protein-coupled receptors. *Anal. Biochem.* **2011**, *409*, 267–272.
- (51) Ligand efficiency $LE = -RT(\ln K_i)/N$, where N is the number of heavy atoms. In the context of the SPR binding affinity data we have substituted K_D for K_i : Hopkins, A. L.; Groom, C. R.; Alex, A. Ligand efficiency: a useful metric for lead selection. *Drug Discovery Today* **2004**, *9*, 430–443.
- (52) Patchett, A. A.; Nargund, R. P. Privileged structures—an update. *Annu. Rep. Med. Chem.* **2000**, *35*, 289–298.
- (53) Lawler, C. P.; Prioleau, C.; Lewis, M. M.; Mak, C.; Jiang, D.; Schetz, J. A.; Gonzalez, A. M.; Sibley, D. R.; Mailman, R. B. Interactions of the novel antipsychotic aripiprazole (OPC-14597) with dopamine and serotonin receptor subtypes. *Neuropsychopharmacology* **1999**, *20*, 612–627.
- (54) Ishiyama, T.; Tokuda, K.; Ishibashi, T.; Ito, A.; Toma, S.; Ohno, Y. Lurasidone (SM-13496), a novel atypical antipsychotic drug, reverses MK-801-induced impairment of learning and memory in the rat passive-avoidance test. *Eur. J. Pharmacol.* **2007**, *572*, 160–170.
- (55) Leeson, P. D.; Springthorpe, B. The influence of drug-like concepts on decision-making in medicinal chemistry. *Nat. Rev. Drug Discovery* **2007**, *6*, 881–890.
- (56) ACD/LogP calculator, version 12.02, within ACD/Chem-Sketch, release 12.00, was used to calculate cLogP values. www.acdlabs.com.
- (57) Mason, J. S.; Bortolato, A.; Congreve, M.; Marshall, F. H. New insights from structural biology into the druggability of G protein-coupled receptors. *Trends Pharmacol. Sci.* **2012**, *33*, 249–260.
- (58) Ballesteros, J. A.; Weinstein, H. Integrated methods for the construction of three-dimensional models and computational probing of structure–function relations in G protein-coupled receptors. *Methods Neurosci.* **1995**, *25*, 366–428.
- (59) To assess aqueous solubility before progression to crystallography trials, **19** and **20** were dissolved in DMSO (to 200 and 150 mM, respectively). Clear solutions resulted after brief sonication and gentle heating. Subsequent 1 in 10 or 1 in 100 aqueous dilutions (10 μ L of DMSO solution plus 90 or 990 μ L of water, respectively) yielded

solutions of 20 and 2 mM. In each case clear solutions were obtained for both compounds.

(60) Warne, T.; Tate, C. G. The importance of interactions with helix 5 in determining the efficacy of β -adrenoceptor ligands. *Biochem. Soc. Trans.* **2013**, *41*, 159–165.

(61) Shoichet, B. K.; Kobilka, B. K. Structure-based drug screening for G-protein-coupled receptors. *Trends Pharmacol. Sci.* **2012**, *33*, 268–272.

(62) Carlsson, J.; Coleman, R. G.; Setola, V.; Irwin, J. J.; Fan, H.; Schlessinger, A.; Sali, A.; Roth, B. L.; Shoichet, B. K. Ligand discovery from a dopamine D₃ receptor homology model and crystal structure. *Nat. Chem. Biol.* **2011**, *7*, 769–778.

(63) Carlsson, J.; Yoo, L.; Gao, Z.-G.; Irwin, J. J.; Shoichet, B. K.; Jacobson, K. A. Structure-based discovery of A_{2A} adenosine receptor ligands. *J. Med. Chem.* **2010**, *53*, 3748–3755.

(64) Kolb, P.; Rosenbaum, D. M.; Irwin, J. J.; Fung, J. J.; Kobilka, B. K.; Shoichet, B. K. Structure-based discovery of β_2 -adrenergic receptor ligands. *Proc. Natl. Acad. Sci. U.S.A.* **2009**, *106*, 6843–6848.

(65) de Graaf, C.; Kooistra, A. J.; Vischer, H. F.; Katritch, V.; Kuijter, M.; Shiroishi, M.; Iwata, S.; Shimamura, T.; Stevens, R. C.; de Esch, I. J. P.; Leurs, R. Crystal structure-based virtual screening for fragment-like ligands of the human histamine H₁ receptor. *J. Med. Chem.* **2011**, *54*, 8195–8206.

(66) Cheng, Y.-C.; Prusoff, W. H. Relationship between the inhibition constant (K_i) and the concentration of inhibitor which causes 50 per cent inhibition (I_{50}) of an enzymatic reaction. *Biochem. Pharmacol.* **1973**, *22*, 3099–3108.

(67) *Maestro*, version 9.1, and *Canvas*, version 1.4; Schrödinger, LLC: New York; <http://www.schrodinger.com>.

(68) Goodford, P. J. A computational procedure for determining energetically favorable binding sites on biologically important macromolecules. *J. Med. Chem.* **1985**, *28*, 849–857.

(69) Sciabola, S.; Stanton, R. V.; Mills, J. E.; Flocco, M. M.; Baroni, M.; Cruciani, G.; Perruccio, F.; Mason, J. S. High-throughput virtual screening of proteins using GRID molecular interaction fields. *J. Chem. Inf. Model.* **2010**, *50*, 155–169.

(70) Bender, A.; Mussa, H. Y.; Glen, R. C. Similarity searching of chemical databases using atom environment descriptors (MOLPRINT 2D): evaluation of performance. *J. Chem. Inf. Comput. Sci.* **2004**, *44*, 1708–1718.

(71) Warne, T.; Serrano-Vega, M. J.; Tate, C. G.; Schertler, G. F. X. Development and crystallization of a minimal thermostabilised G protein-coupled receptor. *Protein Expression Purif.* **2009**, *65*, 204–213.

(72) Warne, T.; Chirside, J.; Schertler, G. F. X. Expression and purification of truncated, non-glycosylated turkey beta-adrenergic receptors for crystallization. *Biochim. Biophys. Acta* **2003**, *1610*, 133–140.

(73) Leslie, A. G. W. The integration of macromolecular diffraction data. *Acta Crystallogr., Sect. D* **2006**, *D62*, 48–57.

(74) Evans, P. Scaling and assessment of data quality. *Acta Crystallogr., Sect. D* **2006**, *D62*, 72–82.

(75) McCoy, A. J.; Grosse-Kunstleve, R. W.; Adams, P. D.; Winn, M. D.; Storoni, L. C.; Read, R. J. Phaser crystallographic software. *J. Appl. Crystallogr.* **2007**, *40*, 658–674.

(76) Murshudov, G. N.; Skubak, P.; Lebedev, A. A.; Pannu, N. S.; Steiner, R. A.; Nicholls, R. A.; Winn, M. D.; Long, F.; Vagin, A. A. REFMAC5 for the refinement of macromolecular crystal structures. *Acta Crystallogr., Sect. D* **2011**, *D67*, 355–367.

(77) Emsley, P.; Lohkamp, B.; Scott, W. G.; Cowtan, K. Features and development of Coot. *Acta Crystallogr., Sect. D* **2010**, *D66*, 486–501.

(78) Davis, I. W.; Leaver-Fay, A.; Chen, V. B.; Block, J. N.; Kapral, G. J.; Wang, X.; Murray, L. W.; Arendall, W. B., 3rd; Snoeyink, J.; Richardson, J. S.; Richardson, D. C. MolProbity: all-atom contacts and structure validation for proteins and nucleic acids. *Nucleic Acids Res.* **2007**, *35*, W375–W383.